LOADING MODE DEPENDENT EFFECTIVE PROPERTIES OF OCTET-TRUSS LATTICE STRUCTURES USING 3D-PRINTING

Adithya Challapalli

Thesis Prepared for the Degree of

MASTER OF SCIENCE

UNIVERSITY OF NORTH TEXAS

May 2015

APPROVED:

Jaehyung Ju, Major Professor
Nandika D'Souza, Committee Member
Xiaohua Li, Committee Member
Yong Tao, Chair of the Department of Mechanical and Energy Engineering
Costas Tsatsoulis, Dean of the College of Engineering and Interim Dean of the Toulouse Graduate School

Challapalli, Adithya. *Loading Mode Dependent Effective Properties of Octet-truss Lattice Structures using 3D Printing.* Master of Science (Mechanical and Energy Engineering), May 2015, 45 pp., 2 tables, 18 figures, 29 numbered references.

Cellular materials, often called lattice materials, are increasingly receiving attention for their ultralight structures with high specific strength, excellent impact absorption, acoustic insulation, heat dissipation media and compact heat exchangers. In alignment with emerging additive manufacturing (AM) technology, realization of the structural applications of the lattice materials appears to be becoming faster. Considering the direction dependent material properties of the products with AM, by directionally dependent printing resolution, effective moduli of lattice structures appear to be directionally dependent. In this paper, a constitutive model of a lattice structure, which is an octet-truss with a base material having an orthotropic material property considering AM is developed. In a case study, polyjet based 3D printing material having an orthotropic property with a 9% difference in the principal direction provides difference in the axial and shear moduli in the octet-truss by 2.3 and 4.6%. Experimental validation for the effective properties of a 3D printed octet-truss is done for uniaxial tension and compression test. The theoretical value based on the micro-buckling of truss member are used to estimate the failure strength. Modulus value appears a little overestimate compared with the experiment. Finite element (FE) simulations for uniaxial compression and tension of octet-truss lattice materials are conducted. New effective properties for the octet-truss lattice structure are developed considering the observed behavior of the octet-truss structure under macroscopic compression and tension trough simulations.

ACKNOWLEDGEMENTS

I would like to express my deepest gratitude to Dr.Jaehyung Ju for being my advisor and steering my research. His support in and out of my research can never be compensated.

I would like to thank Dr. Nandika D’Souza and Dr.Xiaohua Li for being my committee members.

I express my deepest appreciation to Kwangwon Kim, Hyeonu Ho and all my friends for helping me with my research.

TABLE OF CONTENTS

LIST OF TABLES

Page

LIST OF FIGURES

Page

CHAPTER 1

INTRODUCTION

Lattice (or cellular) materials are increasingly receiving attention for their having combinations of mechanical, thermal, and acoustic properties that provide potential opportunities for diverse multifunctional structural applications. Lattice materials offer ultralight structures with high specific strength [1, 2] and high specific strain [3-7], high positive and negative Poisson's ratio [5-7], excellent impact absorption [8, 9], acoustic insulation [10], heat dissipation media and compact heat exchangers [11].

Recent advance in additive manufacturing (AM) allows the production of lattice materials from a variety of constituent materials with high accuracy [10-13].

1.1 Motivation

In spite of the rapidly emerging AM technologies to manufacture complex network cellular geometries, there exists no design tool to integrate process-cell topology(mesostructure)-property, which is the critical gap to move forward to realization of functional parts with cellular structures through AM in industries. For example, products fabricated by the layer-by-layer based AM technologies do not have isotropic properties. Instead, in general, they have orthotropic properties due to the different printing resolutions in the Cartesian coordinates. In addition, depending on the orientation of the part during 3D printing, directionally dependent properties are observed due to the layer-by-layer based manufacturing characteristics of AM, which may limit the scalability of cellular materials to structural applications unless properly designed from their process stage. Moreover, adding reinforcement materials in AM will make the finial structures anisotropic.

1.2 Objective

The objective of this thesis is to develop a constitutive model of a lattice structure having an orthotropic material property of a base material considering AM processes.

In this study, one lattice structure is sought: octet-truss. Constitutive models of octet-truss have been developed by several groups [14-18]. Individual truss members' contribution to the overall stiffness was obtained by three dimensional (3D) coordinate transformations [14-18]. A continuum model with an isotropic property of a base material was also presented [18].

Printing resolution mode	
High Definition (**HD**)	375 x 375 x 790 DPI (xyz); 32µ layers
Ultra High Definition (**UHD**)	750 x 750 x 890 DPI (xyz); 29µ layers
Xtremly High Definition (**XHD**)	750 x 750 x 1600 DPI (xyz); 16µ layers

Figure 1. ProJet HD 300 3D printer

An orthotropic constitutive model of an octet-truss structure is developed with constituent materials' orthotropic properties considering the directionally dependent printing resolution of AM. A continuum based truss model is used to develop the orthotropic properties of the lattice structures. Using the directionally dependent

properties of the base materials, the final products' mechanical properties are estimated. Experimental validation is conducted using a universal testing machine and FE analysis is done using a commercial FE code ABACUS.

Figure 2. Universal testing machine

CHAPTER 2

LITERATURE REVIEW

A lot of research is focused on modeling the truss like space structures and formulating the effective properties of the structures in the past few decades. Different models have been formulated for the mathematical and computational analysis of the truss structures.

Continuum model for three dimensional truss structures are investigated to develop analytical and computational analysis to formulate their equivalent continuum elastic properties by Nayfeh and Hefzy [25]. Octet truss and cubic truss structures are considered in this study. Continuum model is used to write the stress strain equations of the general elastic in the compact form.

$$\sigma_i = C_{ij}\varepsilon_j \tag{i}$$

Where σ_i and ε_j are the independent components of stress and strain respectively.

It was considered that the cubic and the octet-truss are orthotropic. This eliminates $C_{14}, C_{15}, C_{16}, C_{24}, C_{25}, C_{26}, C_{34}, C_{35}, C_{36}, C_{45}, C_{46}\ and\ C_{56}$. Further for a cubic truss structure $C_{13} = C_{12}, C_{33} = C_{11}\ and\ C_{66} = C_{44}$ considering rotational symmetry.

Two different equations are developed for the stiffness matrix of the octet-truss based on its view in two different co-ordinate axis. The node connectivity and the shape of the octet-truss considered in this study is different from the rest of the studies.

A similar continuum model was developed by Mark S. Lake [16]. A crystallographic technique is used to categorize geometric symmetry in the repeated unit cells. The continuum stiffness and failure stresses of the truss are related to the stiffness and failure loads of the members. An equivalent continuum analogy is used for the

analysis of the truss stiffness and strengths. The stiffness in the form of constitutive equations is considered as

$$\begin{Bmatrix} \bar{\sigma}_{11} \\ \bar{\sigma}_{22} \\ \bar{\sigma}_{33} \\ \bar{\sigma}_{23} \\ \bar{\sigma}_{13} \\ \bar{\sigma}_{12} \end{Bmatrix} = \begin{bmatrix} c_{11} & c_{12} & c_{13} & c_{14} & c_{15} & c_{16} \\ c_{21} & c_{22} & c_{23} & c_{24} & c_{25} & c_{26} \\ c_{31} & c_{32} & c_{33} & c_{34} & c_{35} & c_{36} \\ c_{14} & c_{24} & c_{34} & c_{44} & c_{45} & c_{46} \\ c_{15} & c_{25} & c_{35} & c_{45} & c_{55} & c_{56} \\ c_{16} & c_{26} & c_{36} & c_{46} & c_{56} & c_{66} \end{bmatrix} \begin{Bmatrix} \bar{\varepsilon}_{11} \\ \bar{\varepsilon}_{22} \\ \bar{\varepsilon}_{33} \\ 2\bar{\varepsilon}_{23} \\ 2\bar{\varepsilon}_{13} \\ 2\bar{\varepsilon}_{12} \end{Bmatrix} \quad \text{(ii)}$$

and in the form of tensor form as

$$\sigma_{ij} = C_{ijkl}\varepsilon_{kl} \quad \text{(iii)}$$

In this study a characteristic repeating cell that typically possesses geometric symmetry is considers to generate the uniform truss structure similar to a crystalline lattice. Symmetry with respect to the rotational axis are considered for the elastic characteristics of the truss structures. A transformation tensor T_{ij}=$\begin{bmatrix} -1 & 0 & 0 \\ 0 & -1 & 0 \\ 0 & 0 & 1 \end{bmatrix}$ is used to determine the specific rotation in the symmetric axis. This tensor is substituted to find the 21 conditions of the stiffnessC_{ijkl}. Calculations are made using this procedure for cubic, triangular and hexagonal groups.

The stiffness of the entire truss are obtained by summing the stiffness of each of the group of parallel members. The continuum stiffness is calculated by transforming the stiffness of these group of parallel members from local coordinate to global coordinates similar to Nayfeh and Hefzy [25].

$$C_{ijkl} = \sum_n V^{(n)} E_s^{(n)} (T_i T_j T_k T_l) \quad \text{(iv)}$$

here $V^{(n)}\ and\ E_s^{(n)}$ are the volume and the young's modulus of each of the parallel member and $T_i$is the transformational tensor. These equations are used to formulate the

stiffness and strength of the regular octahedral truss structure and isotropic warren structure.

A similar study using the continuum model was conducted by Jong Wan Hu and Park [20] for the plastic deformation of the octet-truss lattice material under multi-axial loading. Homogenization technique is used to transform the components of the truss members from the local coordinate to the global coordinates. Representative volume elements are used to represent the entire lattice structures similar to [25, 16]. To represent the effective properties of the lattice materials and to evaluate the light weight effect of these structures relative density of the lattice structures is used. It is calculated by the ration of the total volume of the truss members in the unit cell to the volume of the unit cell element. FE calculations were made to compare multiaxial loading and analytical results.

Strut-level strengthening and the slenderness ratio related to the geometry of struts is studied to compare between a minimum strengthening design (octet-truss) and a maximum strengthening design (Warren truss) by Doyoyo and Jong Wan Hu [19]. These metallic truss structures are investigated for failure in multi-axial loading. The effects of the stretching and bending in the deformation due to yielding and buckling is studied. Similar continuum model is followed in this study for the effective properties of the truss structures with short struts.

The effective properties of the octet-truss lattice materials were also investigated by Deshpande, Fleck and Ashby [18]. They investigated the properties of stretching dominated cellular materials and compared them with the traditional foam matrix. In this investigation, analytical and FE calculations were reported for the elastic properties and

the collapse surface due to elastic buckling. Experimental validation is done by testing octet-truss material made from an aluminum casting alloy (LM25).

In this study [18], it was stated that the octet-truss structure can be constructed by stacking either the octahedron cell or the tetrahedron cell in the octet structure. The relative density and the effective elastic properties of the octet truss are formulated.

Anisotropic yield criterion using Hills generalization of von Mises yield criterion for materials with orthotropic symmetry is used for expressing the yield criterion. To determine the materials constants, the uniaxial and shear yield strengths are expresses as:

$$\sigma^{y}{}_{xx} = \frac{\sqrt{2}A\,\sigma_x}{2l^2}\,(2)$$

Similarly $$\sigma^{y}{}_{yy} = \frac{\sqrt{2}A\,\sigma_y}{2l^2}\,(2)$$

$$\sigma^{y}{}_{zz} = \frac{\sqrt{2}A\,\sigma_z}{2l^2}\,(2)$$

Similarly $$\sigma^{y}{}_{xy} = \frac{\sqrt{2}A\,\sigma_x}{2l^2}\,(1)$$

$$\sigma^{y}{}_{yz} = \frac{\sqrt{2}A\,\sigma_y}{2l^2}\,(1)$$

$$\sigma^{y}{}_{zx} = \frac{\sqrt{2}A\,\sigma_z}{2l^2}\,(1) \qquad \text{(v)}$$

here $\sigma^{y}{}_{xx} \ldots \sigma^{y}{}_{zx}$ are the Uni-axial and shear strengths of the truss elements $\sigma_x \ldots \sigma_z$ are the stresses of the entire structure, *A* is the area and *l* is the length of the truss elements.

Analysis for the elastostatic specific stiffness of 2D stretching dominated lattice materials is done by Elsayed and Pasini [26]. This analysis is used to define for the stretching dominated and bending dominated behavior of the materials. In this study the Cauchy-Born hypothesis is used to find the microscopic lattice nodal deformation in terms

of macroscopic strain field of the material. This is used to find the microscopic element deformation in the terms of macroscopic strain field. The microscopic element deformation in the terms of macroscopic strain field derives the properties of the material macroscopic stiffness. Lattice structures with structural elements extending between adjacent unit cells are dealt by with introducing dummy node scheme. Further analysis on the stiffness and strength of tridimensional periodic lattice structures by Vigliotti and Pasini [27]. In this analysis, a multi-scale approach is adopted which is separated in to two scales of lattice analysis. A macro scale level in which the stiffness of the lattice component is determined the structure as a uniform continuum. At the micro scale level, the stiffness and the internal forces of each element is calculated as both are essential for the analysis of the lattice strength. In this analysis, stresses callused by the macroscopic stress field in each of the truss element is calculated to verify the occurrence of the yielding and buckling failure at the micro scale level.

In this study, the orthotropic effective properties and strengths are developed for an octet-truss lattice structure considering the compression and tension phenomenon of each of the truss element. Experimental and simulation validation are also presented.

Table 1

Previous research concentration on lattice structures

Author- Title	Effective Properties Isotropic	Effective Strengths	Experimental Validation	FE Analysis
Nayfeh and Hefzy Continuum Modeling of 3-Dimentional Truss-like Space Structures	Yes	No	No	No
Mark S. Lake Stiffness and Strength Tailoring in Uniform Truss Structures	Yes	No	No	No
Deshpande, Fleck, Ashby Effective Properties of Octet-lattice Material	Yes	Yes	Yes	Yes
Doyoyo, Jong Wan Multi-axial failure of lattice materials with short and slender struts	No	Yes	No	Yes
Vigliotti, Pasini Stiffness and strength of tridimensional lattices	Yes	Yes	No	No
Jing Wan, Park Continuum Model for Plastic Deformation of Octet-truss Lattice Materials Under Multiaxial Loading	Yes	No	No	Yes

2.1 Stress-Strain Relations [28]

The general case of stress-strain components generalized by Hooks law contains 81 elastic constants. The symmetry of the stress and strain tensors reduces the 81 components in to 36 ($\sigma_{ij} = \sigma_{ji,}\ \varepsilon_{ij} = \varepsilon_{ji}$). This gives the stress-strain relation of anisotropic body as

$$\begin{Bmatrix}\sigma_1\\ \sigma_2\\ \sigma_3\\ \tau_4\\ \tau_5\\ \tau_6\end{Bmatrix} = \begin{bmatrix}c_{11} & c_{12} & c_{13} & c_{14} & c_{15} & c_{16}\\ c_{21} & c_{22} & c_{23} & c_{24} & c_{25} & c_{26}\\ c_{31} & c_{32} & c_{33} & c_{34} & c_{35} & c_{36}\\ c_{14} & c_{24} & c_{34} & c_{44} & c_{45} & c_{46}\\ c_{15} & c_{25} & c_{35} & c_{45} & c_{55} & c_{56}\\ c_{16} & c_{26} & c_{36} & c_{46} & c_{56} & c_{66}\end{bmatrix}\begin{Bmatrix}\varepsilon_1\\ \varepsilon_2\\ \varepsilon_3\\ \gamma_4\\ \gamma_5\\ \gamma_6\end{Bmatrix}$$

$$\begin{Bmatrix}\varepsilon_1\\ \varepsilon_2\\ \varepsilon_3\\ \gamma_4\\ \gamma_5\\ \gamma_6\end{Bmatrix} = \begin{bmatrix}s_{11} & s_{12} & s_{13} & s_{14} & s_{15} & s_{16}\\ s_{21} & s_{22} & s_{23} & s_{24} & s_{25} & s_{26}\\ s_{31} & s_{32} & s_{33} & s_{34} & s_{35} & s_{36}\\ s_{14} & s_{24} & s_{34} & s_{44} & s_{45} & s_{46}\\ s_{15} & s_{25} & s_{35} & s_{45} & s_{55} & s_{56}\\ s_{16} & s_{26} & s_{36} & s_{46} & s_{56} & s_{66}\end{bmatrix}\begin{Bmatrix}\sigma_1\\ \sigma_2\\ \sigma_3\\ \tau_4\\ \tau_5\\ \tau_6\end{Bmatrix} \quad \text{(vi)}$$

The 36 components are reduced in to 9 components in the case of an orthotropic material due to various stiffness and compliance terms are related to each other.

$$\begin{Bmatrix}\sigma_1\\ \sigma_2\\ \sigma_3\\ \tau_4\\ \tau_5\\ \tau_6\end{Bmatrix} = \begin{bmatrix}c_{11} & c_{12} & c_{13} & 0 & 0 & 0\\ c_{21} & c_{22} & c_{23} & 0 & 0 & 0\\ c_{31} & c_{32} & c_{33} & 0 & 0 & 0\\ 0 & 0 & 0 & c_{44} & 0 & 0\\ 0 & 0 & 0 & 0 & c_{55} & 0\\ 0 & 0 & 0 & 0 & 0 & c_{66}\end{bmatrix}\begin{Bmatrix}\varepsilon_1\\ \varepsilon_2\\ \varepsilon_3\\ \gamma_4\\ \gamma_5\\ \gamma_6\end{Bmatrix}$$

$$\begin{Bmatrix}\varepsilon_1\\ \varepsilon_2\\ \varepsilon_3\\ \gamma_4\\ \gamma_5\\ \gamma_6\end{Bmatrix} = \begin{bmatrix}s_{11} & s_{12} & s_{13} & 0 & 0 & 0\\ s_{21} & s_{22} & s_{23} & 0 & 0 & 0\\ s_{31} & s_{32} & s_{33} & 0 & 0 & 0\\ 0 & 0 & 0 & s_{44} & 0 & 0\\ 0 & 0 & 0 & 0 & s_{55} & 0\\ 0 & 0 & 0 & 0 & 0 & s_{66}\end{bmatrix}\begin{Bmatrix}\sigma_1\\ \sigma_2\\ \sigma_3\\ \tau_4\\ \tau_5\\ \tau_6\end{Bmatrix} \quad \text{(vii)}$$

The octet-truss have eight tetrahedrons. Each tetrahedron can be replicated and packed with mirror planes or rotation to each axis by 90^0. This mirror symmetry reduces the 9 components in to 3 elastic components [20].

$$\begin{Bmatrix}\sigma_1\\ \sigma_2\\ \sigma_3\\ \tau_4\\ \tau_5\\ \tau_6\end{Bmatrix} = \begin{bmatrix}c_{11} & c_{12} & c_{13} & 0 & 0 & 0\\ c_{21} & c_{22} & c_{23} & 0 & 0 & 0\\ c_{31} & c_{32} & c_{33} & 0 & 0 & 0\\ 0 & 0 & 0 & c_{44} & 0 & 0\\ 0 & 0 & 0 & 0 & c_{55} & 0\\ 0 & 0 & 0 & 0 & 0 & c_{66}\end{bmatrix}\begin{Bmatrix}\varepsilon_1\\ \varepsilon_2\\ \varepsilon_3\\ \gamma_4\\ \gamma_5\\ \gamma_6\end{Bmatrix} \quad \text{(viii)}$$

Where $c_{11} = c_{22} = c_{33}$, $c_{12} = c_{13} = c_{21} = c_{23} = c_{31} = c_{32}$, $c_{44} = c_{55} = c_{66}$

Table 2

Rotational symmetry-elastic characteristics

No.	Conditions on continuum stiffness	Independent elastic constants
1	No symmetry (General Anisotropic Material)	81
2	$\sigma_{ij} = \sigma_{ji}$, $\varepsilon_{ij} = \varepsilon_{ji}$	36
3	Orthotropic material	9
4	Transversely isotropic material ($C_{12} = C_{13}$; $C_{22} = C_{33}$)	6
		3

2.2 Buckling Strength [29]

The theory of simply supported straight column subjected to axial loading, first developed by Leonard Euler obtains the differential equation as

$$EI\frac{d^2v}{dx^2} + Pv = 0 \quad \text{(ix)}$$

Where *E* is the young's modulus, *I* is the moment of inertia, *P* is the axial load and v is the displacement.

Applying the boundary conditions v (0) =0, v (L) =0 and solving for *P* gives

$$P_n = \frac{n^2\pi^2 EI}{L^2}, \text{ n=1, 2, 3…} \quad \text{(x)}$$

Here *L* is the length of the column.

The lowest value at which the buckling occurs is when n=1 is the critical buckling load or the Euler's load

$$P_{cr} = \frac{\pi^2 EI}{L^2} \quad \text{(xi)}$$

The end conditions, i.e. the support to the column effects the buckling load.

$$P_{cr} = \frac{\pi^2 EI}{{L^2}_{eff}} \quad \text{(xii)}$$

Here ${L^2}_{eff}$ depends on the type of end condition.

The critical buckling strength can be written as

$$\sigma_{cr}^{(k)} = \frac{P_{cr}}{A} = \left(\frac{\pi^2 E_s^{(k)} I}{{L^2}_{eff}}\right)\frac{1}{A} \quad \text{(xiii)}$$

CHAPTER 3

CONSTITUTIVE MODELING OF ORTHOTROPIC OCTET-TRUSS

In this section, effective modulus and effective strength of octet-truss is developed for a base material whose property is orthotropic, resulting in an orthotropic property of octet-truss.

3.1 Lattice Material (Octet-truss)

A lattice material is constructed by stacking unit-cells which repeat in the orthogonal direction. The unit cell element behaves as a representative volume element and still possesses overall physical properties of the bulk lattice. The unit cell of octet-truss consists of eight identical tetrahedron elements, in which each tetrahedron is a combination of one octet and one diagonal sub-lattice element as shown in Figure 1. The tetrahedron can be considered the sub-unit cell for constructing an octet-truss structure. The sub-unit cell consists of six truss members: Each truss member has a length of $\sqrt{2}L$ and a cross-sectional area, $A^{(k)}$ (Figure 3).

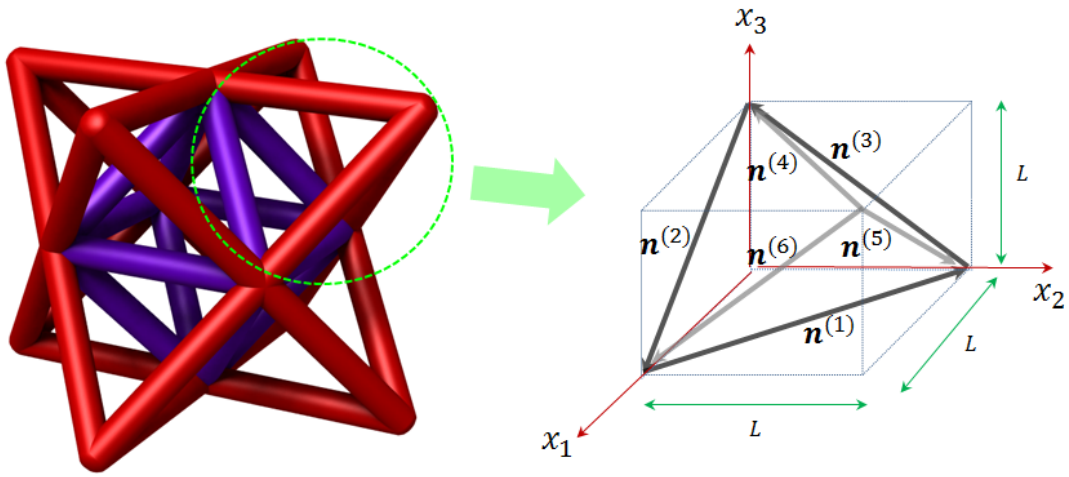

Figure 3. Octet-truss structure and unit cell

3.2 Unit Normal Direction

In Figure 3, unit normal directions, $n^{(k)}$ of the six truss members are obtained from the transformation of the global coordinate systems to the local coordinates:

$$\mathrm{n}^{(1)} = \frac{1}{\sqrt{2}}\hat{e}_x + \frac{1}{\sqrt{2}}\hat{e}_y$$

$$\mathrm{n}^{(2)} = \frac{1}{\sqrt{2}}\hat{e}_x + \frac{1}{\sqrt{2}}\hat{e}_z$$

$$\mathrm{n}^{(3)} = \frac{1}{\sqrt{2}}\hat{e}_y + \frac{1}{\sqrt{2}}\hat{e}_z$$

$$\mathrm{n}^{(4)} = \frac{1}{\sqrt{2}}\hat{e}_x + \frac{1}{\sqrt{2}}\hat{e}_y$$

$$\mathrm{n}^{(5)} = \frac{1}{\sqrt{2}}\hat{e}_x + \frac{1}{\sqrt{2}}\hat{e}_z$$

$$\mathrm{n}^{(6)} = \frac{1}{\sqrt{2}}\hat{e}_y + \frac{1}{\sqrt{2}}\hat{e}_z \qquad (1)$$

The superscript (k) indicates each truss member in the subunit cell.

3.3 Representative Volume Element (RVE)

The representative volume element (RVE), a continuum element with a statistical ensemble of micro scale objects, corresponds to the unit cell in the periodic medium [19]. The lattice materials composed of the truss members at the micro scale level are considered as the averaged continuum medium at the macroscopic level. The average stress $\overline{\sigma}$ in the global coordinate system is obtained by volume averaging the local stress σ in the local coordinate systems over the volume of the RVE.

$$\overline{\sigma} = \frac{1}{V}\int_V \sigma^{(k)} \mathrm{N}\, dV \tag{2}$$

where N denotes the linear transformation operator from the local to the global coordinates. Note that each truss member in the unit cell has its own orientation. Therefore, every local orientation of the truss members should be transformed in the global orientation through N in order to formulate the macro scale continuum theory.

$$\begin{aligned}\overline{\sigma} &= \frac{1}{V}\sum_{k=1}^{N} N_{ij}^{(k)} \sigma^{(k)} V^{(k)} \\ &= \frac{1}{V}\sum_{k=1}^{N} N_{ij}^{(k)} \sigma^{(k)} A^{(k)} l^{(k)}\end{aligned} \tag{3}$$

where $A^{(k)}$ and $l^{(k)}$ are the cross sectional area and the length of truss members, respectively.

Considering a linear elastic relation using Hooke's law at the local truss elements, the average stress in the global coordinates is expressed as

$$\overline{\sigma} = \frac{1}{V}\sum_{k=1}^{N} N_{ij}^{(k)} E_s^{(k)} \varepsilon^{(k)} V^{(k)} \tag{4}$$

where $E_s^{(k)}$ denotes Young's modulus of the k^{Th} truss member. Note that only axial stiffness $E_s^{(k)}$ of truss members was considered in Equation (4) in the truss lattice

materials because bending and shear modes of truss members are negligible compared with axial stiffness$E_s^{(k)}$.

$\varepsilon^{(k)}$, the microscale strain in the local coordinates and $\bar{\varepsilon}$, the macroscale strain in the global coordinates are correlated as

$$\varepsilon^{(k)} = N_{kl}^{(k)}\bar{\varepsilon} \tag{5}$$

Inserting Equation (5) into Equation (4) provides the macroscopic constitutive relationship of lattice structures:

$$\bar{\sigma} = \frac{1}{V}\sum_{k=1}^{n} V^{(k)} E_s^{(k)} N_{ij}^{(k)} N_{kl}^{(k)} \bar{\varepsilon} \tag{6}$$

Therefore, the macroscopic stiffness tensor C for the unit cell is expressed as

$$\begin{aligned} C_{ijkl} &= \frac{1}{V}\sum_{k=1}^{n} V^{(k)} E_s^{(k)} N_{ij}^{(k)} N_{kl}^{(k)} \\ &= \frac{1}{V}\sum_{k=1}^{n} V^{(k)} E_s^{(k)} \left(n_i^{(k)} \cdot n_j^{(k)}\right)\left(n_k^{(k)} \cdot n_l^{(k)}\right) \\ &= \frac{1}{V}\sum_{k=1}^{n} A^{(k)} l^{(k)} E_s^{(k)} \left(n_i^{(k)} \cdot n_j^{(k)}\right)\left(n_k^{(k)} \cdot n_l^{(k)}\right) \\ &= \frac{1}{V}\sum_{k=1}^{n} A\, l\, E_s^{(k)} \left(n_i^{(k)} \cdot n_j^{(k)}\right)\left(n_k^{(k)} \cdot n_l^{(k)}\right) \\ &= \frac{A\, l}{V}\sum_{k=1}^{n} E_s^{(k)} \left(n_i^{(k)} \cdot n_j^{(k)}\right)\left(n_k^{(k)} \cdot n_l^{(k)}\right) \end{aligned} \tag{7}$$

Now, considering constituent materials' anisotropic property which may be caused during the process of AM: for example, different extruding and feeding speeds at Fused Deposition Modeling (FDM), different laser (or electron) beam scanning and feeding speeds at selective laser (or electron) melting systems, different scanning and feeding speeds at stereo-lithography, etc. Those produce varying resolution in the principal directions, resulting in a varying mechanical property; e.g. modulus and strength. Adding

reinforcing materials is challenging to predict the mechanical properties of lattice structures in terms of material's anisotropic (often orthotropic) property.

Embedding anisotropy into each truss member in the local coordinate may have two cases in the general additive manufacturing: One is the case that we know the material properties in the global coordinate is known and apply local orientation. Global scanning at stereo-lithography may be an example of this case.

The other is that one may know the material property in the local coordinate and apply transformation from local to global coordinate. FDM with reinforced materials and selective laser (or electron) melting systems are the examples of this case. In this study, focus is laid on the former case considering our manufacturing method – direct light processing (DLP) which is a stereo-lithography.

3.4 Effective Modulus

First, mechanical properties of each of the truss members are evaluated, when the mechanical properties in the global coordinate system is known.

Considering materials orthotropic properties by additive manufacturing process, $E_s^{(k)}$ can be expressed as

$$E_s^{(k)} = \mathrm{n}^{(k)} \cdot \hat{\mathrm{e}}_x (E_s)_x + \mathrm{n}^{(k)} \cdot \hat{\mathrm{e}}_y (E_s)_y + \mathrm{n}^{(k)} \cdot \hat{\mathrm{e}}_z (E_s)_z \qquad (8)$$

where $(E_s)_x$, $(E_s)_y$, and $(E_s)_z$ are the moduli in the x, y, and z directions of the global coordinate system by possible mismatch of the resolution in the principal direction.

The corresponding orthotropic moduli of each truss member are expressed as

$$E_s^{(1)} = \cos^2\theta (E_s)_x + \sin^2\theta (E_s)_y$$

$$E_s^{(2)} = \cos^2\theta (E_s)_x + \sin^2\theta (E_s)_z$$

$$E_s^{(3)} = \cos^2\theta (E_s)_y + \sin^2\theta (E_s)_z$$

$$E_s^{(4)} = \cos^2\theta(E_s)_x + \sin^2\theta(E_s)_y$$

$$E_s^{(5)} = \cos^2\theta(E_s)_x + \sin^2\theta(E_s)_z$$

$$E_s^{(6)} = \cos^2\theta(E_s)_y + \sin^2\theta(E_s)_z \quad (9)$$

where θ is the angle between the unit normal directions, $\mathrm{n}^{(k)}$ of the six truss members and the basis of the principal coordinate.

From Equations (6) and (9), the macroscopic constitutive equation of orthotropic octet-truss is developed:

$$\begin{Bmatrix} \bar{\sigma}_{11} \\ \bar{\sigma}_{22} \\ \bar{\sigma}_{33} \\ \bar{\sigma}_{23} \\ \bar{\sigma}_{13} \\ \bar{\sigma}_{12} \end{Bmatrix} = \frac{\pi r^2}{4\sqrt{2}L^2} \begin{bmatrix} c_{1111} & c_{1122} & c_{1133} & 0 & 0 & 0 \\ c_{2211} & c_{2222} & c_{2233} & 0 & 0 & 0 \\ c_{3311} & c_{3322} & c_{3333} & 0 & 0 & 0 \\ 0 & 0 & 0 & c_{2323} & 0 & 0 \\ 0 & 0 & 0 & 0 & c_{1313} & 0 \\ 0 & 0 & 0 & 0 & 0 & c_{1212} \end{bmatrix} \begin{Bmatrix} \bar{\varepsilon}_{11} \\ \bar{\varepsilon}_{22} \\ \bar{\varepsilon}_{33} \\ 2\bar{\varepsilon}_{23} \\ 2\bar{\varepsilon}_{13} \\ 2\bar{\varepsilon}_{12} \end{Bmatrix} \quad (14)$$

where

$$c_{1111} = E_s^{(1)} + E_s^{(2)} + E_s^{(4)} + E_s^{(5)}$$

$$c_{2222} = E_s^{(1)} + E_s^{(3)} + E_s^{(4)} + E_s^{(6)}$$

$$c_{3333} = E_s^{(2)} + E_s^{(3)} + E_s^{(5)} + E_s^{(6)}$$

$$c_{1122} = c_{2211} = E_s^{(1)} + E_s^{(4)}$$

$$c_{1133} = c_{3311} = E_s^{(2)} + E_s^{(5)}$$

$$c_{2233} = c_{3322} = E_s^{(3)} + E_s^{(6)}$$

$$c_{2323} = E_s^{(3)} + E_s^{(6)}$$

$$c_{1313} = E_s^{(2)} + E_s^{(5)}$$

$$c_{1212} = E_s^{(1)} + E_s^{(4)}$$

There are nine independent elastic constants in Equation (14) compared with three in octet-truss with an isotropic material [18].

Note that because each truss member shares its half the cross sectional area with the one in the adjacent unit cell, the volume of each truss member in the unit-cell, $V^{(k)}$ is $\frac{\sqrt{2}}{2}\pi r^2 L$ considering a half part of the circular cross sectional area of the truss members whose radii are *r* ($A^{(k)} = \frac{1}{2}\pi r^2$) and the length of the truss members ($l^{(k)}$=$\sqrt{2}L$). The volume of the unit cell $V(= L^3)$ is equal toL^3. The relative density of lattice materials ρ^* is defined as the ratio of the density of the lattice material to the density of the constituent material ($\rho^* = \rho/\rho_s$) which is nothing but the volume fraction of the truss members in the unit cell ($V^{(k)}/V$). This provides the relative density of $3\sqrt{2}\pi\left(\frac{r}{L}\right)^2$ in the octet-truss, which is a function of r and L.

3.5 Effective Strengths

The failure strength of octet-truss $\overline{\sigma}_f$ can also be expressed with a base material's anisotropy together with each truss member's local orientation. Knowing the strength of the base material in the principal directions in the global coordinate, the effective strength of the octet-truss is obtained by

$$\overline{\sigma}_f = \frac{1}{V}\sum_{k=1}^{N} N_{ij}^{(k)}\sigma_f^{(k)}V^{(k)} \tag{15}$$

where $\sigma_f^{(k)}$ is the strength at of the k^{th} truss member.

Alternatively, Equation (15) can be expressed as

$$\left(\sigma_f^*\right)_{ij} = \frac{1}{V}\sum_{k=1}^{N} N_{ij}^{(k)}\sigma_f^{(k)}V^{(k)}$$

$$= \frac{1}{V}\sum_{k=1}^{N} n_i^{(k)} \cdot n_j^{(k)}\sigma_f^{(k)}V^{(k)}$$

$$= \frac{1}{V}\sum_{k=1}^{N} n_i^{(k)} \cdot n_j^{(k)} \sigma_f^{(k)} A^{(k)} l^{(k)}$$

$$= \frac{1}{V}\sum_{k=1}^{N} n_i^{(k)} \cdot n_j^{(k)} \sigma_f^{(k)} A\, l$$

$$= \frac{A\, l}{V}\sum_{k=1}^{N} n_i^{(k)} \cdot n_j^{(k)} \sigma_f^{(k)} \tag{16}$$

The corresponding orthotropic strengths of each of the truss elements are as following

$$\sigma_f^{(k)} = \mathrm{n}^{(k)} \cdot \hat{\mathrm{e}}_x(\sigma)_x + \mathrm{n}^{(k)} \cdot \hat{\mathrm{e}}_y(\sigma)_y + \mathrm{n}^{(k)} \cdot \hat{\mathrm{e}}_z(\sigma)_z$$

$$\sigma_f^{(1)} = \cos^2\theta(\sigma)_x + \sin^2\theta(\sigma)_y$$

$$\sigma_f^{(2)} = \cos^2\theta(\sigma)_x + \sin^2\theta(\sigma)_z$$

$$\sigma_f^{(3)} = \cos^2\theta(\sigma)_y + \sin^2\theta(\sigma)_z$$

$$\sigma_f^{(4)} = \cos^2\theta(\sigma)_x + \sin^2\theta(\sigma)_y$$

$$\sigma_f^{(5)} = \cos^2\theta(\sigma)_x + \sin^2\theta(\sigma)_z$$

$$\sigma_f^{(6)} = \cos^2\theta(\sigma)_y + \sin^2\theta(\sigma)_z \tag{16a}$$

The effective strengths of the octet-truss under tension or compression can be expressed by substituting the respective strengths of the truss elements.

$$\left(\sigma_f^*\right)_{11} = \frac{\pi r^2}{2\sqrt{2}L^2}\left[\sigma_f^{(1)} + \sigma_f^{(2)} + \sigma_f^{(4)} + \sigma_f^{(5)}\right]$$

$$\left(\sigma_f^*\right)_{22} = \frac{\pi r^2}{2\sqrt{2}L^2}\left[\sigma_f^{(1)} + \sigma_f^{(3)} + \sigma_f^{(4)} + \sigma_f^{(6)}\right]$$

$$\left(\sigma_f^*\right)_{33} = \frac{\pi r^2}{2\sqrt{2}L^2}\left[\sigma_f^{(2)} + \sigma_f^{(3)} + \sigma_f^{(5)} + \sigma_f^{(6)}\right]$$

$$\left(\sigma_f^*\right)_{12} = \frac{\pi r^2}{2\sqrt{2}L^2}\left[\sigma_f^{(1)} + \sigma_f^{(4)}\right]$$

$$\left(\sigma_f^*\right)_{23} = \frac{\pi r^2}{2\sqrt{2}L^2}\left[\sigma_f^{(3)} + \sigma_f^{(6)}\right]$$

$$\left(\sigma_f^*\right)_{13}=\frac{\pi r^2}{2\sqrt{2}L^2}\left[\sigma_f^{(2)}+\sigma_f^{(5)}\right] \quad (16b)$$

If the octet-truss is under compression, the base material is brittle and the aspect ratio of the truss members is low (number), we may regard the failure mode as micro-buckling of truss members.

3.6 Buckling Strength

The octet-truss material collapses by elastic buckling of the truss members if the Euler buckling strength, $\sigma_{cr}^{(k)}$ in the truss member is less than their plastic yield strength,$\sigma_Y^{(k)}$. $\sigma_{cr}^{(k)}$ in the truss member can be expressed as

$$\sigma_{cr}^{(k)}=\frac{P_{cr}}{A}=\left(\frac{n^2\pi^2E_s^{(k)}I}{l^2}\right)\frac{1}{A}=\frac{n^2\pi^2E_s^{(k)}}{l^2}\frac{\pi r^4}{4}\frac{1}{\pi r^2}=\frac{n^2\pi^2E_s^{(k)}}{4}\left(\frac{r}{l}\right)^2 \quad (17)$$

where I is the second area moment of inertia of the truss members. The factor n depends on the rotational stiffness of the end nodes the truss member. We simplify the problem with $n=1$ because the strut buckles at the smallest buckling load, P_{cr} for which buckling is possible.

CHAPTER 4

CASE STUDY

In this section, the model developed in Section II with 3D printed octet-truss structure is validated. First the base material's anisotropy induced by direction dependent fabrication resolution is characterized. Then, the corresponding anisotropy on the macroscopic modulus and strength of octet-truss is checked.

4.1 Constituent Material

As a basis on the overall design of lattice structures, base materials' mechanical properties need to be characterized as a function of process control parameters. A direct light process (DLP) based 3D printer (ProJet^{TM} HD3500 Plus, 3D Systems) with an extremely high resolution is used. The extremely high definition (XHD) mode has 750, 750, and 1600 Drop per Inch (DPI) in the x, y, z directions, respectively, with a dimensional accuracy of 0.1%.

Considering the microscopic compression stress of the all truss members of the octet-truss for a uniaxial macroscopic compression, we prepare three photopolymer (VisiJet Procast) samples with varying printing orientation for tensile test of a dumbbell shaped sample (Figure 2a, $a = 33mm$, $b = 115mm$, $t = 2mm$) according to ASTM D412 and compression test of a cylindrical sample ($diameter = 12.7mm, lengh = 25.4mm$) (Figure 3a)according to ASTM D575. An electromechanical material testing system (Criterion C43.104, MTS) was used with 2 and 10kN load cells for tensile and compression tests, respectively.

The compression results show that samples A and B oriented in the x and y directions, respectively, have a similar mechanical behavior (Figure 5 (b)). Sample C

which is oriented in the z direction has a lower modulus. Measured values are as follows;$(E_s)_x = 1.21GPa$, $(E_s)_y = 1.22GPa$ and $(E_s)_z = 1.17GPa$. This is an interesting result. One may think that sample C should have higher modulus considering the higher printing resolution in the z direction. However, this idea makes one clear. Considering a specific resolution factor, α, which is a relative resolution in the z direction compared to the x and y directions, the volume of sample C is $\frac{D^2}{4}(\alpha L)$. On the other hand, the volumes of samples A and B are $\frac{(\alpha D)^2}{4}L$. Interestingly, if the shape of samples changes, e.g., a cubic shape, the volume density will be αl^3 regardless of the orientation.

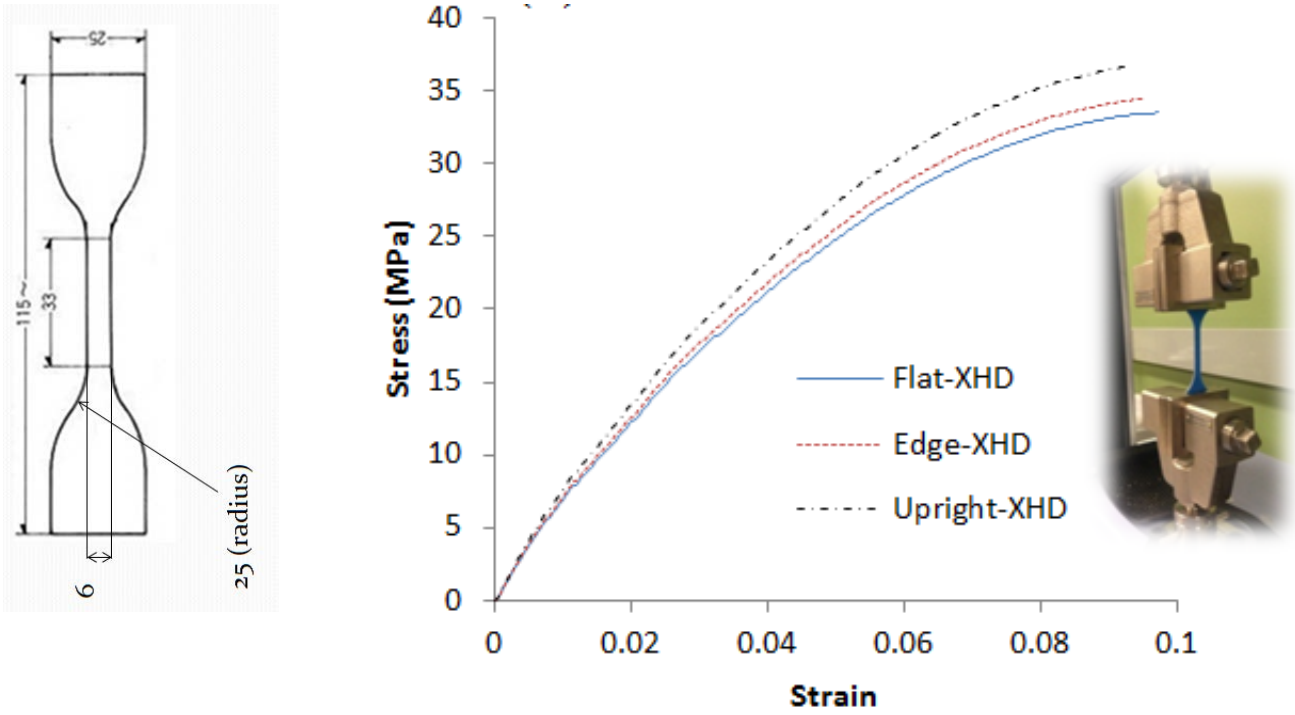

Figure 4. Uniaxial tensile stress-strain curves of the base material as a function printing orientation (strain rate 0.001/s)

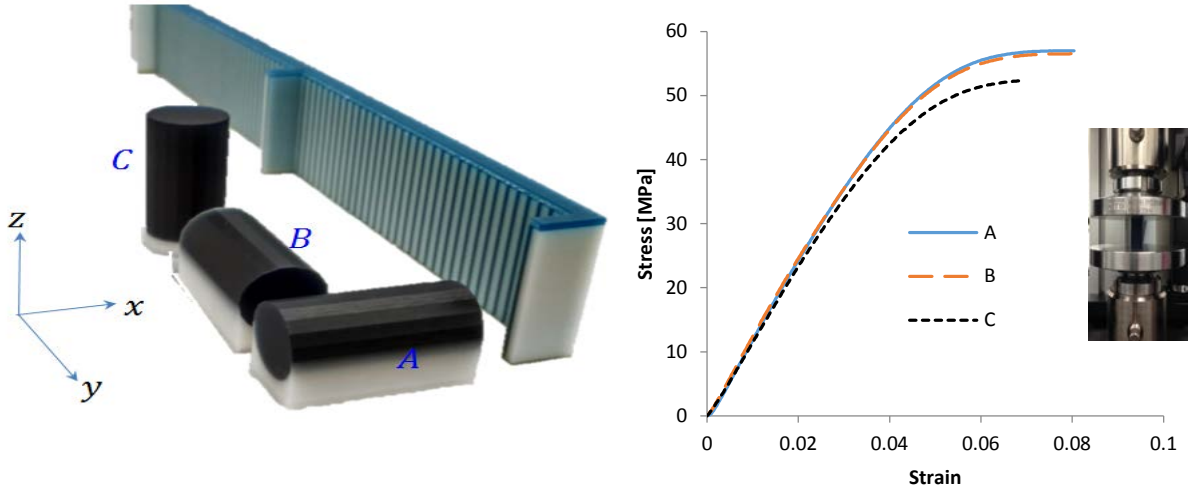

(a) samples with varying printing orientation

(b) Stress-strain curves

Figure 5. Uniaxial compressive stress-strain curves of the base material as a function printing orientation (strain rate 0.001/s)

4.2 Parametric Study

4.2.1 Octet-truss Effective Modulus

Effective moduli in the normal direction of the octet-truss structure as a function of the relative density can be obtained from Equation (14) and are plotted in Figure 5. A linear relationship in the effective modulus of octet-truss in the every principal axial direction is obtained as a function of relative density. The effective moduli of octet-truss in the *x* direction, E_{11} $(= E_{22})$, are 26.82 and 107.30MPa for relative densities of 0.133 (for $r/L = 0.25$) and 0.533 (for $r/L = 0.5$), respectively. The effective modulus of octet-truss in the *z* direction, E_{33} is are slightly lower than the corresponding values of E_{11} $(= E_{22})$; 26.55 and 106.18MPa for relative densities of 0.133 and 0.533 respectively. The difference between E_{33} and E_{11} $(= E_{22})$ are only about 2.3%.

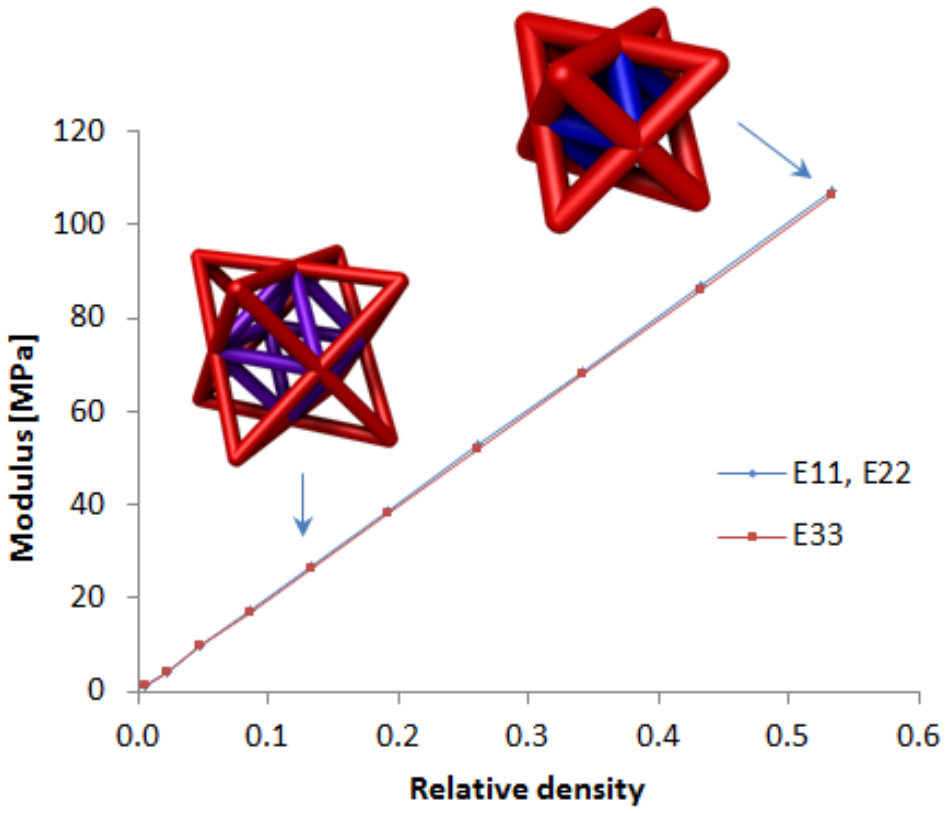

Figure 6. Effective moduli of the octet-truss for uniaxial loading

4.2.2 Octet-truss Shear Modulus

Effective shear moduli of the octet-truss structure as a function of relative density are plotted in Figure 6. A linear relationship in the effective shear modulus of octet-truss in the every principal direction is also obtained as a function of relative density. G_{23} (= G_{31}) values are 13.27 and 53.09MPa for relative densities of 0.133 and 0.533, respectively. A slightly higher shear modulus is obtained with G_{12}. The G_{12} values are 13.55 and 54.2MPa for the relative densities of 0.133 and 0.533, respectively. The difference between G_{23} $(= G_{13})$ and G_{12} are only about 4.6%, which is higher than the difference in the axial moduli.

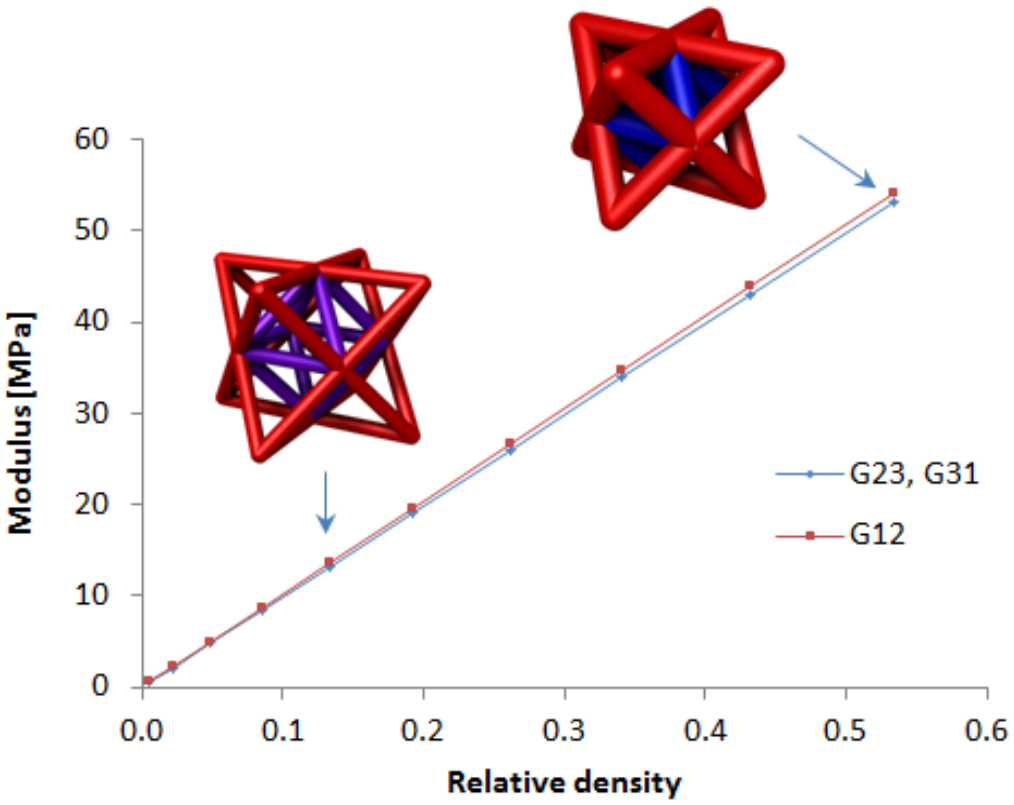

Figure 7. Effective shear moduli of octet-truss

Even though the difference (~9%) in the moduli of the base materials exists, slight difference (2.3%) in the axial moduli of the octet-truss is obtained. Difference in shear moduli is higher (4.6%) than that of axial moduli, but it still appears to be marginal.

4.2.3 Octet-truss Effective Strength Under Uni-axial Loading

Strength values of octet-truss in the in uniaxial loading in the principal direction show a nonlinear relationship with relative density (Figure 8).

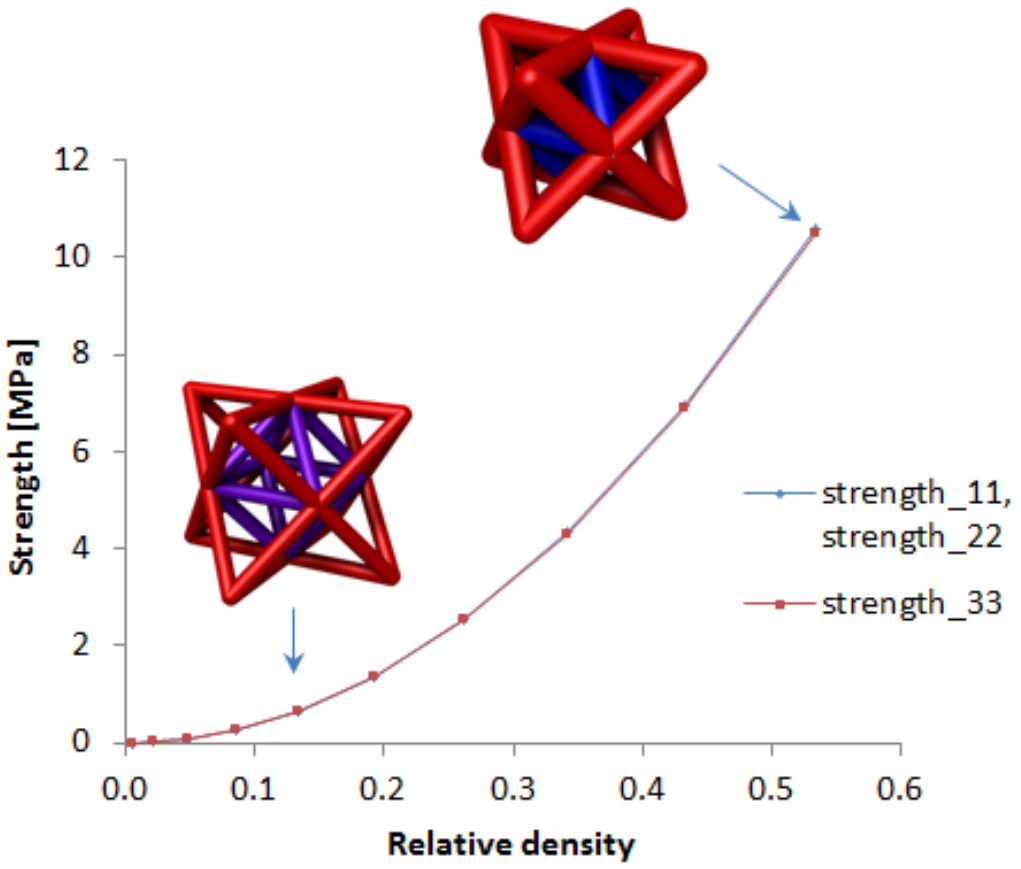

Figure 8. Effective strength of the octet-truss lattice material for uniaxial loading in the principal directions

4.2.4 Octet-truss Shear Strength Under Uni-axial Loading

Figure 9 shows the strength of octet-truss materials for shear loading as a function of relative density. The shear strength of the octet-truss material shows a quadratic increase with the relative density.

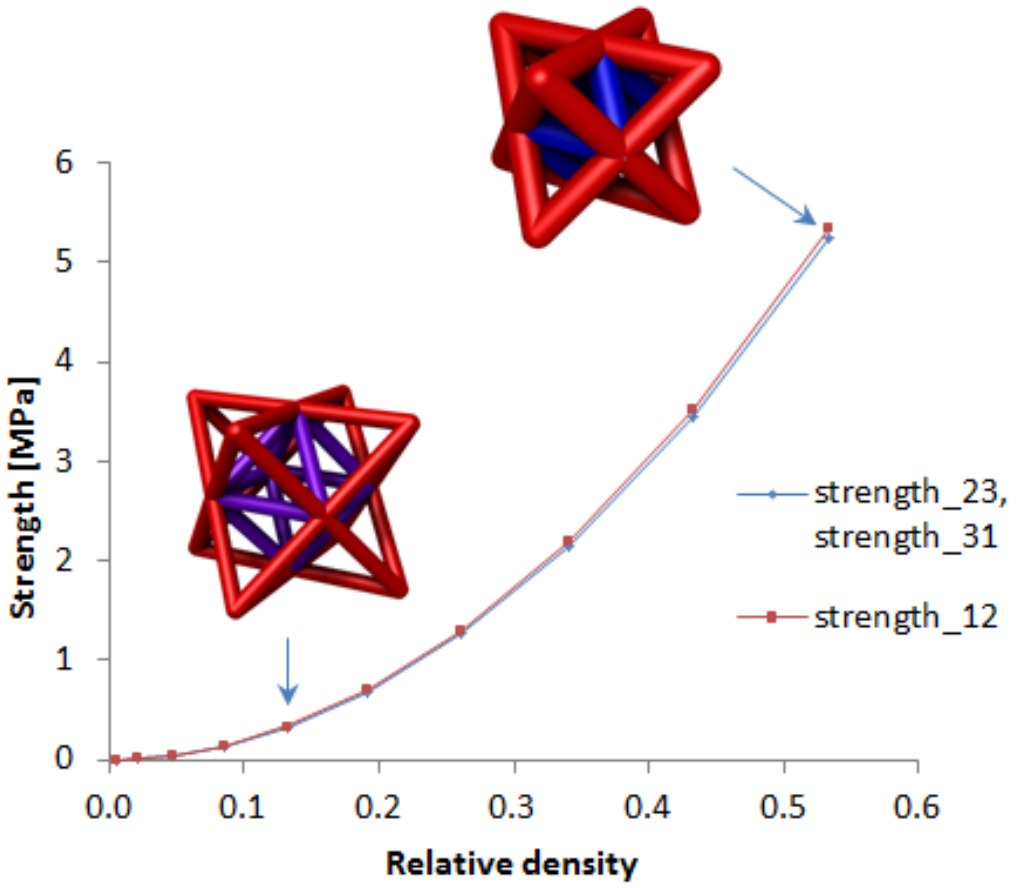

Figure 9. Effective strength of the octet-truss materials for shear loading in the principal direction

Wallach and Gibson reported direction dependent properties of a lattice material for varying aspect ratio of the unit cell – the ration of cell height to cell width [24]. In their study, they showed that modulus and strength values decrease in certain directions. It is worthwhile to note that we fix the aspect ratio of the unit cell and observed the effective properties with varying radius of strut members, resulting in varying the relative density.

CHAPTER 5

EXPERIMENT

For experimental validation of the effective properties of octet-truss, uniaxial compression test with a 3D printed octet-truss with a photo-polymer (Procast, 3D Systems) as shown in Figure 6a is conducted. A $25 \times 25 \times 25mm^3$ cubic octet-truss lattice material is prepared. A cylindrical truss (radius $r = 0.25mm$ and length $l = 5\sqrt{2}mm$) is used. Octet-truss lattice materials 3D printed in different direction were prepared for uniaxial loading tests – 3D printed in the x and z direction (Figure 7). It should be noted that loading in the y direction should be the same as that in the x-direction.

Uniaxial tests of the octet-truss lattice material were conducted in the two principal directions – the x and z directions.

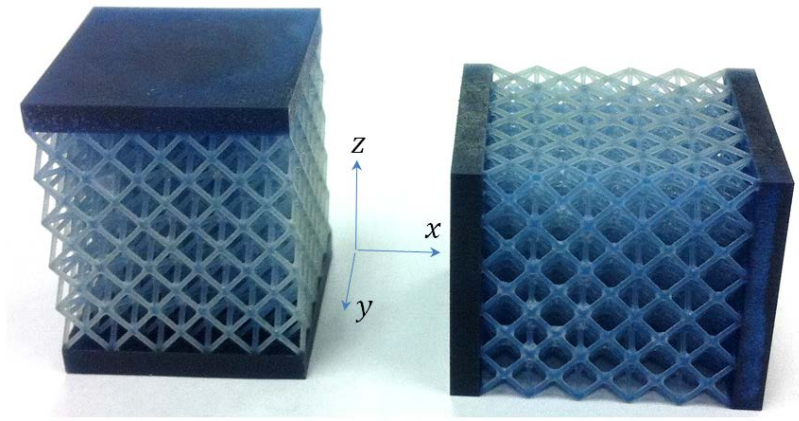

Figure 10. Octet-truss lattice materials 3D printed in the vertical (z) and horizontal (x) directions

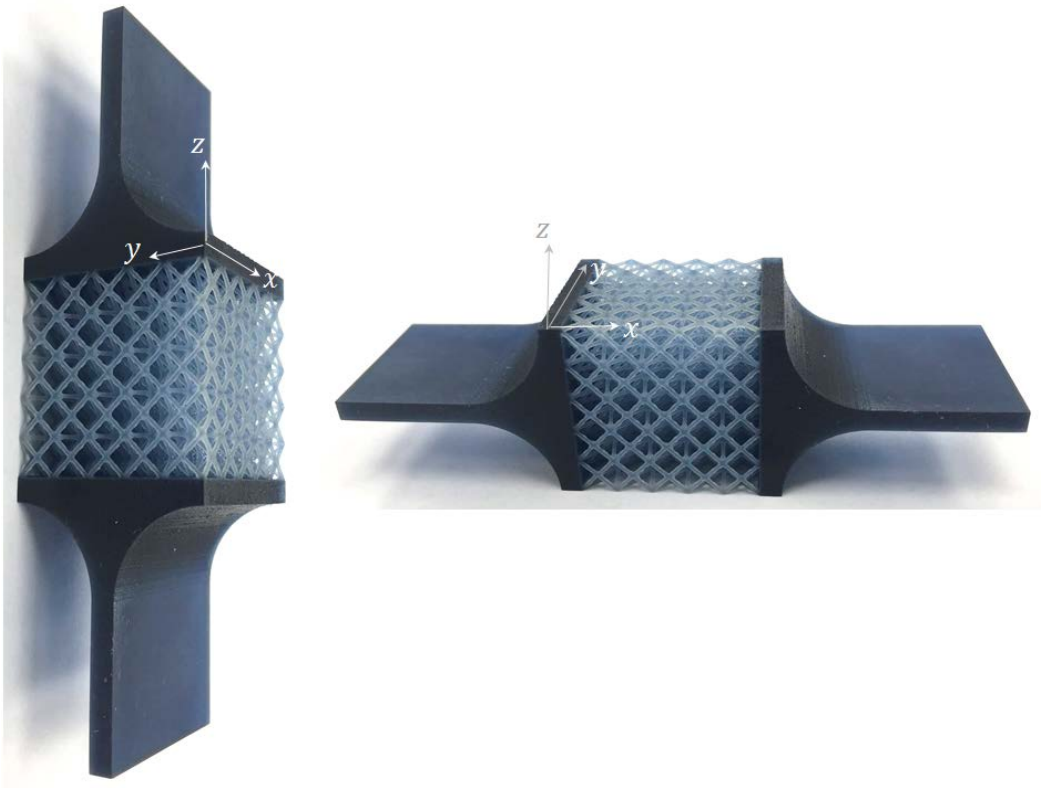

Figure 11. Octet-truss lattice materials 3D printed in the vertical (z) and horizontal (x) directions

It shows a brittle failure mode by a micro-buckling of the truss members (Figure 7b). The failure plains are located on the orthogonal directions oriented at $45°$ from the principal direction (Figure 6b).

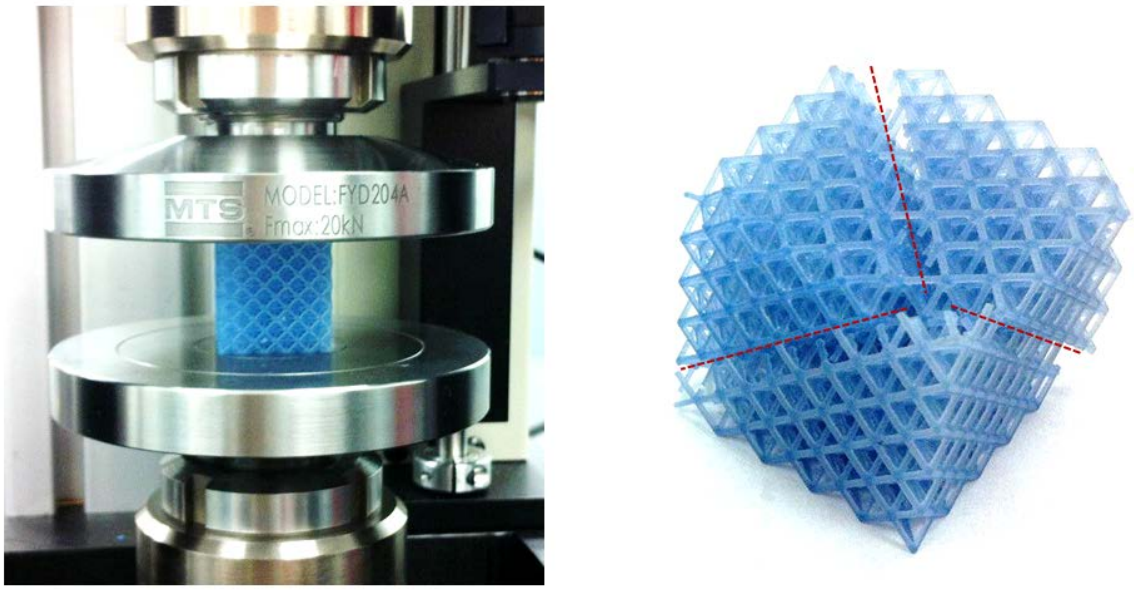

Figure 12. Uniaxial compression test setup for an octet-truss with relative density of 0.133 and failure shape

5.1 Experimental vs. Theoretical

Figure 13 shows macroscopic stress-strain curves of the octet-truss lattice material with direction dependent material property by 3D printing orientation (horizontal - x and vertical –z directions) under uniaxial compressive loading. Modulus and strength of the octet-truss material for uniaxial compressive loading in the x-direction are 21.52MPa and 0.57MPa, respectively. A lower value in modulus and strength were obtained with the octet-truss lattice material for uniaxial compressive loading in the z-direction; 18.58MPa and 0.47MPa for modulus and strength, respectively. This is due to the lower value in modulus and strength of the base material in z direction as observed in Figure 5b.

For comparison, the curve generated from Equations (14) and (18) was presented as well. The theoretical value based on the micro-buckling of truss member predicts the failure strength well. However, modulus value from Equation (14) appears to a little overestimate compared with the experiment.

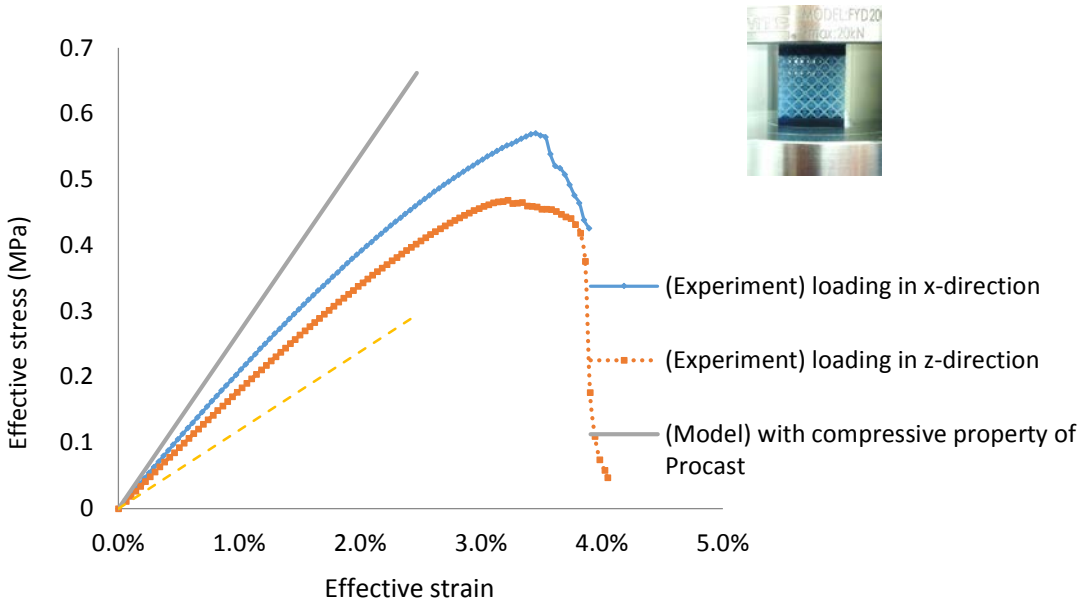

Figure 13. Macroscopic compressive stress-strain curves of the octet-truss with a relative density of 0.133

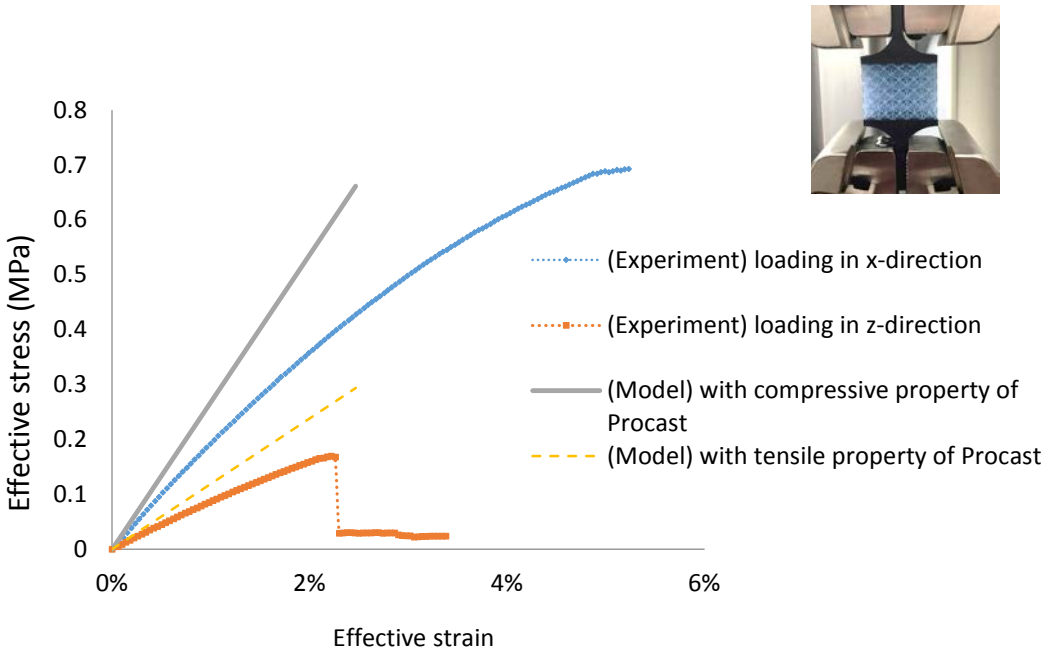

Figure 14. Macroscopic tension stress-strain curves of the octet-truss with a relative density of 0.133

CHAPTER 6

FINITE ELEMENT SIMULATION

Finite element (FE) simulations on uniaxial loading (both compression and tension) of octet-truss lattice materials were conducted. A commercial FE code, ABAQUS, was used for the simulation. A 3 node quadratic 3D truss element (T3D3 in ABAQUS) was used to construct the truss members for the lattice structure. The bottom nodes of the octet-truss structures were fixed for translation in the x_3 direction and rotation with respect to the x_1, x_2, and x_3 directions. The bottom center node was fixed both in translation and rotation. A displacement loading in the x_3 direction was applied at the top nodes.

6.1 Uni-axial Compression

The loading behavior under macroscopic compression, the lateral members are in tension in a microscopic view (Figure 15). On the other hand, the diagonal members are in a compression mode microscopically.

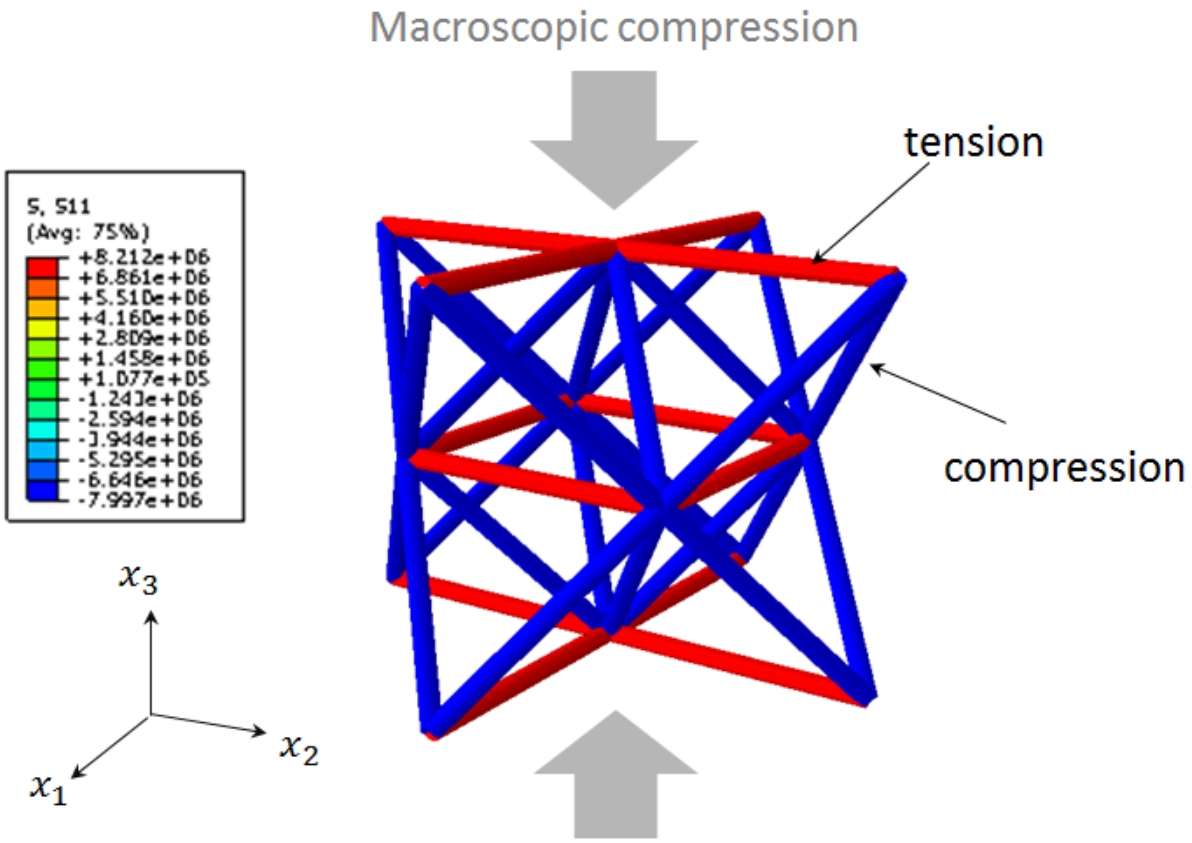

Figure 15. FE simulation of octet-truss under compression

6.2 Uni-axial Tension

Observing the behavior of the octet-truss under macroscopic tension, the members in the lateral direction with respect to the load direction are in compression (Figure 16). On the other hand, the diagonal members are in tension.

This shows that microscopic members are in mixed mode even though a single macroscopic uniaxial is applied (Figures 15 and 16). This means that modulus ($E_s^{(k)}$) and strength ($\sigma_f^{(k)}$) of the solid should be separately applied when build the macroscopic constitutive model of the octet-truss depending on the loading mode, if the property of the solid is clearly different in tension and compression.

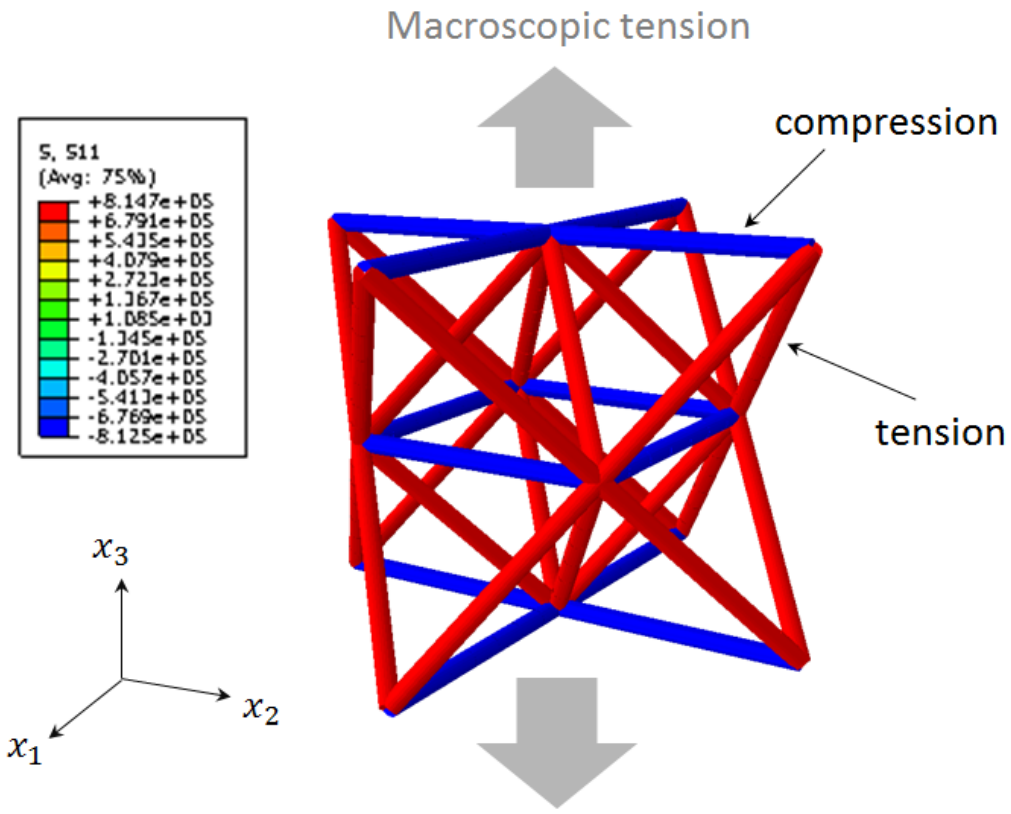

Figure 16. FE simulation of octet-truss under tension

CHAPTER 7

MODIFIED PROPERTIES OF OCTET-TRUSS

7.1 Modified Effective Properties

The effective properties of the octet-truss considering the microscopic mixed mode for compression and tension properties based on the simulation results can be modified as

7.1.1 Modulus of Truss Elements for Uni-axial Tension

For uniaxial tension, the truss members 1 and 4 are in compression and the rest of the members (2, 3, 5, and 6) are in tension.

$$E_s^{(1)} = \cos^2\theta(E_{cs})_x + \sin^2\theta(E_{cs})_y$$

$$E_s^{(2)} = \cos^2\theta(E_{ts})_x + \sin^2\theta(E_{ts})_z$$

$$E_s^{(3)} = \cos^2\theta(E_{ts})_y + \sin^2\theta(E_{ts})_z$$

$$E_s^{(4)} = \cos^2\theta(E_{cs})_x + \sin^2\theta(E_{cs})_y$$

$$E_s^{(5)} = \cos^2\theta(E_{ts})_x + \sin^2\theta(E_{ts})_z$$

$$E_s^{(6)} = \cos^2\theta(E_{ts})_y + \sin^2\theta(E_{ts})_z \quad (18a)$$

7.1.2 Modulus of Truss Elements for Uni-axial Compression

For uniaxial compression, the truss members 1 and 4 are in tension and the rest of the members (2, 3, 5, and 6) are in compression.

$$E_s^{(1)} = \cos^2\theta(E_{ts})_x + \sin^2\theta(E_{ts})_y$$

$$E_s^{(2)} = \cos^2\theta(E_{cs})_x + \sin^2\theta(E_{cs})_z$$

$$E_s^{(3)} = \cos^2\theta(E_{cs})_y + \sin^2\theta(E_{cs})_z$$

$$E_s^{(4)} = \cos^2\theta(E_{ts})_x + \sin^2\theta(E_{ts})_y$$

$$E_s^{(5)} = \cos^2\theta(E_{cs})_x + \sin^2\theta(E_{cs})_z$$

$$E_s^{(6)} = \cos^2\theta(E_{cs})_y + \sin^2\theta(E_{cs})_z \quad (18b)$$

here E_{cs} is the modulus of the core material for compression and E_{ts} is the modulus of the core material for tension.

The final macroscopic constitutive equation of the octet-truss with the modified effective properties can be formulated by using the modified effective properties as

$$\begin{Bmatrix} \bar{\sigma}_{11} \\ \bar{\sigma}_{22} \\ \bar{\sigma}_{33} \\ \bar{\sigma}_{23} \\ \bar{\sigma}_{13} \\ \bar{\sigma}_{12} \end{Bmatrix} = \frac{\pi r^2}{4\sqrt{2}L^2} \begin{bmatrix} c_{1111} & c_{1122} & c_{1133} & 0 & 0 & 0 \\ c_{2211} & c_{2222} & c_{2233} & 0 & 0 & 0 \\ c_{3311} & c_{3322} & c_{3333} & 0 & 0 & 0 \\ 0 & 0 & 0 & c_{2323} & 0 & 0 \\ 0 & 0 & 0 & 0 & c_{1313} & 0 \\ 0 & 0 & 0 & 0 & 0 & c_{1212} \end{bmatrix} \begin{Bmatrix} \bar{\varepsilon}_{11} \\ \bar{\varepsilon}_{22} \\ \bar{\varepsilon}_{33} \\ 2\bar{\varepsilon}_{23} \\ 2\bar{\varepsilon}_{13} \\ 2\bar{\varepsilon}_{12} \end{Bmatrix} \quad (19)$$

$$c_{1111} = E_s^{(1)} + E_s^{(2)} + E_s^{(4)} + E_s^{(5)}$$

$$c_{2222} = E_s^{(1)} + E_s^{(3)} + E_s^{(4)} + E_s^{(6)}$$

$$c_{3333} = E_s^{(2)} + E_s^{(3)} + E_s^{(5)} + E_s^{(6)}$$

$$c_{1122} = c_{2211} = E_s^{(1)} + E_s^{(4)}$$

$$c_{1133} = c_{3311} = E_s^{(2)} + E_s^{(5)}$$

$$c_{2233} = c_{3322} = E_s^{(3)} + E_s^{(6)}$$

$$c_{2323} = E_s^{(3)} + E_s^{(6)}$$

$$c_{1313} = E_s^{(2)} + E_s^{(5)}$$

$$c_{1212} = E_s^{(1)} + E_s^{(4)}$$

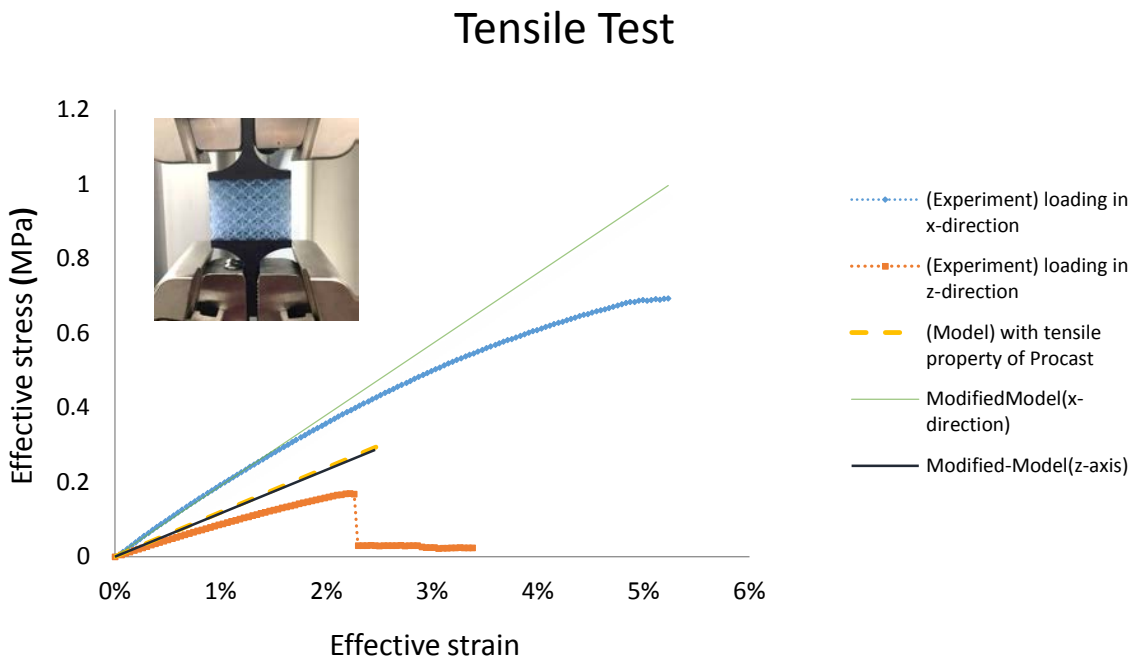

Figure 17. Modified compressive stress-strain curves of the octet-truss

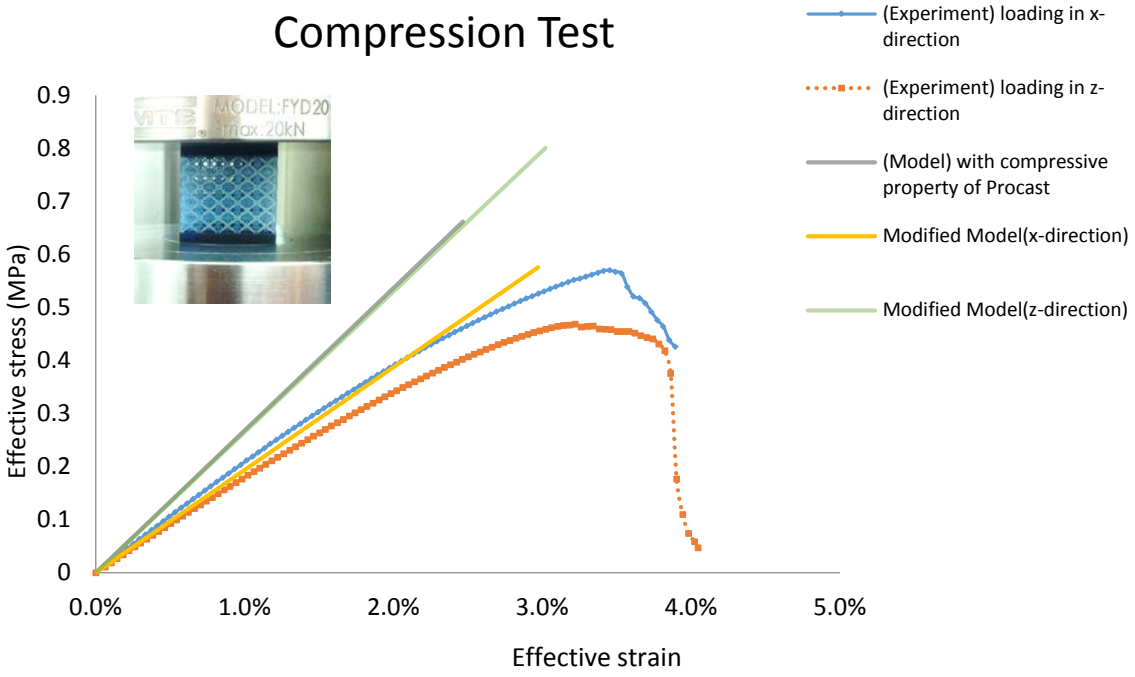

Figure 18. Modified tension stress-strain curves of the octet-truss

7.2 Modified Effective Strengths

The effective crushing strengths by micro-bucking considering the mixed mode properties can be modified by replacing $E_s^{(k)}$ (modulus) of the truss members 1 and 4 with E_{ts} (modulus of core material for tension) and $E_s^{(k)}$ (modulus) of the truss members 2, 3, 5 and 6 with E_{cs} (modulus of core material for compression) in the Euler buckling strength ($\sigma_{cr}^{(k)}$).

7.2.1 Strength of Truss Elements for Uni-axial Tension

The strengths of each of the truss elements for the octet-truss under tension can be expressed as

$$\sigma_f^{(1)} = \cos^2\theta(\sigma_{cr})_x + \sin^2\theta(\sigma_{cr})_y$$

$$\sigma_f^{(2)} = \cos^2\theta\left(\sigma_{tf}\right)_x + \sin^2\theta\left(\sigma_{tf}\right)_z$$

$$\sigma_f^{(3)} = \cos^2\theta\left(\sigma_{tf}\right)_y + \sin^2\theta\left(\sigma_{tf}\right)_z$$

$$\sigma_f^{(4)} = \cos^2\theta(\sigma_{cr})_x + \sin^2\theta(\sigma_{cr})_y$$

$$\sigma_f^{(5)} = \cos^2\theta\left(\sigma_{tf}\right)_x + \sin^2\theta\left(\sigma_{tf}\right)_z$$

$$\sigma_f^{(6)} = \cos^2\theta\left(\sigma_{tf}\right)_y + \sin^2\theta\left(\sigma_{tf}\right)_z \quad \text{(20a)}$$

7.2.2 Strength of Truss Elements for Uni-axial Compression

The strengths of each of the truss elements for the octet-truss under compression can be expressed as

$$\sigma_f^{(1)} = \cos^2\theta\left(\sigma_{tf}\right)_x + \sin^2\theta\left(\sigma_{tf}\right)_y$$

$$\sigma_f^{(2)} = \cos^2\theta(\sigma_{cr})_x + \sin^2\theta(\sigma_{cr})_z$$

$$\sigma_f^{(3)} = \cos^2\theta(\sigma_{cr})_y + \sin^2\theta(\sigma_{cr})_z$$

$$\sigma_f^{(4)} = \cos^2\theta\left(\sigma_{tf}\right)_x + \sin^2\theta\left(\sigma_{tf}\right)_y$$

$$\sigma_f^{(5)} = \cos^2\theta(\sigma_{cr})_x + \sin^2\theta(\sigma_{cr})_z$$

$$\sigma_f^{(6)} = \cos^2\theta(\sigma_{cr})_y + \sin^2\theta(\sigma_{cr})_z \ . \qquad (20b)$$

CHAPTER 8

CONCLUSION REMARKS

Considering orthotropic properties caused by AM process, constitutive relations were developed using a continuum model with a homogenization technique. Effective strengths are also formulated considering an octet-truss structure. As a case study, a polyjet based 3D printing materials with an orthotropic property with a 9% difference in the principal direction, difference in the axial and shear moduli are small; 2.3 and 4.6%.

For the experimental validation of the effective properties of octet-truss, uniaxial compression test are conducted with a 3D printed octet-truss with a photo-polymer (Procast, 3D Systems). It was observed that a brittle failure mode by a micro-buckling of the truss members occurs. The failure plains are located on the orthogonal directions oriented at $45°$ from the principal direction. For comparison, the curves generated for the effective properties and elemental strengths were presented as well. The theoretical value based on the micro-buckling of truss member predicts the failure strength well. However, modulus value appears to a little overestimate compared with the experiment.

Finite element (FE) simulations on uniaxial loading (both compression and tension) of octet-truss lattice materials is conducted. It was observed that for the loading behavior under macroscopic compression, the lateral members are in tension in a microscopic view. On the other hand, the diagonal members are in a compression mode microscopically.

Observing the behavior of the octet-truss under macroscopic tension, the members in the lateral direction with respect to the load direction are in compression. On the other hand, the diagonal members are in tension. New effective modulus and strengths for the

octet-truss lattice structure were developed considering the observed behavior of the octet-truss structure under macroscopic compression and tension.

REFERENCES

[1] Gibson L.J. and Ashby, M. F., 1997, Cellular Solids-Structure and Properties *Cambridge University Press*, Cambridge, UK

[2] Ju, J. and Summers, J.D., 2011, Compliant Hexagonal Periodic Lattice Structures Having Both High Shear Strength and High Shear Strain *Materials & Design*, 32(2):512-524

[3] Ju, J., Summers, J.D., Ziegert, J., and Fadel, G., 2012, Design of Honeycombs for Modulus and Yield Strain in Shear *Journal of Engineering Materials and Technology*, 134(1):011002

[4] Heo, H., Ju, J., Kim, D.-M., 2013, Compliant Cellular Structures: Application to a Passive Morphing Airfoil *Composite Structures*, 106:560-569

[5] Kim, K., Ju, J., Kim, D.-M., 2013, Porous Materials with High Negative Poisson's Ratios – A Mechanism Based Material Design *Smart Materials and Structures*, 22:084007

[6] Kim, K., Lee, J., Ju, J., and Kim, D.-M., 2014, Compliant Cellular Materials with Compliant Porous Structures: A Mechanism Based Materials Design *International Journal of Solids and Structures*, 51(21):3889-3903

[7] Lee, J., Kim, K., Ju, J., and Kim, D.-M., 2014, Compliant Cellular Materials with Elliptical Holes: Materials Design with Mechanisms *Journal of Engineering Materials and Technology*, 131(1):011001

[8] Tan, H. and Qu, S., 2010, Chap 6: Impact of Cellular Materials *Cellular and Porous Materials in Structures and Processes*, *CISM International Centre for Mechanical Science, Springer*.

[9] Schultz, J., Griese, D., Ju, J., Shankar, P., Summers, J.D., and Thompson, L., 2012, Design of Honeycomb Meso-Structures for Crushing Energy Absorption *Journal of Mechanical Design,* 134(7):071004

[10] Phani, A. S., Woodhouse, J., Fleck, N.A., 2006, Wave Propagation in Two-Dimensional Periodic Lattices *Journal of Acoustical Society of America*, 119(4):1995-2005.

[11] Kumar, R. S., and McDowell, D.L., 2004, Rapid Preliminary Design of Rectangular Linear Cellular Alloys for Maximum Heat Transfer *AIAA Journal*, 42(8):1652-1661

[12] Kruth, J.P., Leu, M.C., Nakagawa, T., 1998, Progress in Additive Manufacturing and Rapid Prototyping *CIRP Annals – Manufacturing Technology*, 47(2):525-540

[13] Gibson, I. , Rosen, D.W., Stucker, B., 2010, *Additive Manufacturing Technologies - Rapid Prototyping to Direct Digital Manufacturing*, Springer

[14] Bourell, D.L. and Beaman, Jr. J. J, 2012, The History of Laser Additive Manufacturing *Laser Institute of America*.

[15] Lipson, H. and Kurman, M., 2013, Fabricated: The New World of 3D Printing, Wiley

[16] Lake, M.S., 1992, Stiffness and Strength Tailoring in Uniform Space-Filling Truss Structures *NASA TP-3210.*

[17] Christensen, R.M., 2000, Mechanics of Cellular and Other Low Density Materials *International Journal of Solids and Structure.* 37: 93-104*.*

[18] Deshpande, V.S., Fleck, N.A. and Ashby, M.F., 2001, Effective Properties of Octet-truss Lattice Materials *Journal of mechanics and physics of solids,* 49: 1747-1769.

[19] Doyoyo, M. and Hu, J.W., 2006, Plastic Failure Analysis of an Auxetic Foam of Inverted Strut Lattice under Longitudinal and Shear loads *Journal of Mechanics and Physics of Solids*, 54(7):1479-1492.

[20] Hu, J. W., Park, T., 2013, Continuum Models for the Plastic Deformation of Octet-Truss Lattice Materials under Multiaxial Loading *Transactions of the ASME: Journal of Engineering Materials and Technology,* 135:021004.

[21] Hill, R, 1963, Elastic Properties of Reinforced Solis: Some Theoretical Principles *Journal of the Mechanics and Physics of Solids*, 11(5):357-372

[22] ASTM (tensile)

[23] ASTM (compression)

[24] Wallach, J.C., Gibson, L.J., 2001, Mechanical Behavior of a Tree-Dimensional Truss Material *International Journal of Solids and Structures*, 38:7181-7196

[25] Adnan H.Nayfeh, Mohamed S. Hefzy, Continuum Modeling for Three Dimensional Truss-Like structures *AIAA Journal,* Vo 16, No., Aug 1978*.*

[26] Mostafa Elsayed, Damiano Pasini, Analysis of the elastostatic specific stiffness of 2D stretching dominated lattice materials *Computational methods in applied mechanics and engineering,* 229-232(2012) 27-3*.*

[27] Andrea Vigliotti, Damiano Pasini, Stiffness and Strength of Tridimensional Periodic Lattice *Mechanics of Materials* 42 (2010) 709–725.

[28] Isaac M. Daniel, Engineering Mechanics of Composite Materials *Oxford University Press.*

[29] Vable, *Mechanics of Materials*, 2010.